

Lattice Thermal Transport in Two-Dimensional Alloys and Fractal Heterostructures

Aravind Krishnamoorthy¹, Nitish Baradwaj¹, Aiichiro Nakano¹, Rajiv K. Kalia¹, and Priya Vashishta^{1,*}

¹Collaboratory for Advanced Computing and Simulations, University of Southern California, Los Angeles, CA 90089
*priyav@usc.edu

ABSTRACT

Engineering thermal transport in two dimensional materials, alloys and heterostructures is critical for the design of next-generation flexible optoelectronic and energy harvesting devices. Direct experimental characterization of lattice thermal conductivity in these ultra-thin systems is challenging and the impact of dopant atoms and hetero-phase interfaces, introduced unintentionally during synthesis or as part of deliberate material design, on thermal transport properties is not understood. Here, we use non-equilibrium molecular dynamics simulations to calculate lattice thermal conductivity of (Mo|W)Se₂ monolayer crystals including Mo_{1-x}W_xSe₂ alloys with substitutional point defects, periodic MoSe₂|WSe₂ heterostructures with characteristic length scales and scale-free fractal MoSe₂|WSe₂ heterostructures. Each of these features has a distinct effect on phonon propagation in the crystal, which can be used to design fractal and periodic alloy structures with highly tunable thermal conductivities. This control over lattice thermal conductivity will enable applications ranging from thermal barriers to thermoelectrics.

Introduction

Two dimensional semiconductors are an important class of functional nanomaterials with promising electronic and mechanical properties for optoelectronic and thermoelectric applications. Monolayer transition metal dichalcogenides of composition AB₂ (A = Mo/W and B = S/Se/Te) have recently attracted a lot of attention for optoelectronic properties arising from their favorable electronic band gaps in the range of 1.0 - 2.0 eV, high charge-carrier mobilities and large on/off ratios¹⁻⁴. Thermal engineering of these monolayered materials remains a challenge for the design of devices based on two-dimensional materials. For instance, materials for thermal barrier coatings and thermoelectric energy generation require tight control over phonon transport over a wide range of frequencies to achieve minimal thermal conductivities⁵, whereas materials for optoelectronic devices, where thermal dissipation is key, have opposing design requirements.⁶ Extensive efforts have been made to develop monolayered materials for thermoelectric applications, where a low lattice thermal conductivity is essential for achieving a high figure of merit⁷⁻⁹. While several two-dimensional and layered materials have been characterized experimentally and computationally for their thermal transport properties¹⁰⁻¹², a systematic understanding of the role of point and extended defects and interfaces on controlling thermal conductivity in these systems is lacking.

However, several previous experimental and theoretical investigations have attempted to modulate lattice thermal transport in these material systems by a combination of alloying, interfacial and microstructural engineering and phase patterning. Alloying modifies thermal transport in materials by affecting one or more of the following material parameters – crystal structure, atomic mass¹³, inter-atomic bonding and anharmonicity^{14,15} and is effective in scattering high-frequency phonons⁵. Formation of interfaces and superlattice structures in nanomaterials are very promising for controlling phonon scattering, particularly for low frequency phonons over 1-2 THz¹⁶⁻²⁰. Scale-invariant fractal patterning, which results in features of multiple sizes, are widely pursued to affect phonons over a wide range of frequencies and mean free paths²¹. These panoscopic techniques for hierarchical-design have been applied to identify electron-crystal and phonon-glass materials with excellent thermoelectric properties²².

In this study, we use non-equilibrium molecular dynamics simulations (Section) to compute lattice thermal conductivity of monolayer (Mo|W)Se₂ systems, including Mo_{1-x}W_xSe₂ alloys (Section) and fractal heterostructures (Section) and periodic superlattices (Section) constructed out of two transition metal dichalcogenides, MoSe₂ and WSe₂, suitable for ultra-thin electronic applications. This distribution of point defects, hetero-phase interfaces and a range of feature sizes allows us to explore the influence of each of these features on phonon scattering and identify guidelines for design of two-dimensional material structures with tunable thermal transport properties.

Results

Non-Equilibrium Molecular Dynamics Simulations for Computing Thermal Conductivity of (Mo|W)Se₂ Layers

Lattice thermal conductivity (κ_{lat}) of suspended monolayer crystals is computed using the so-called ‘direct’ method of non-equilibrium molecular dynamics simulations (Figure 1a). This non-perturbative approach for the calculation of κ_{lat} for a heterogeneous system, is consistent with values extracted from classical equilibrium MD (EMD) simulations using Green-Kubo techniques²³, but does not suffer from deficiencies in the commonly adopted relaxation time approximation solutions to the Boltzmann Transport Equation, which are known to severely underpredict the thermal conductivity of several 2D materials including transition metal dichalcogenides^{24,25}. To compute the κ_{lat} for thermal transport along the x direction in a (Mo|W)Se₂ monolayer of dimensions $2L \times L$, a predefined flux of thermal energy, \dot{Q} , is added to the atoms in a 100 Å-strip at $x = \frac{L}{2}$ (‘Hot’ end) and an identical heat flux is removed from the system at $x = \frac{3L}{2}$ (‘Cold’ end). Periodic boundary conditions along the x - and y -directions, ensure an equal magnitude of thermal flux in the x and $-x$ directions from the ‘Hot’ to the ‘Cold’ ends. The thermal conductivity of the system can then be obtained directly from the steady-state temperature gradient using the Fourier law of heat conduction (Equation 1).

$$\kappa_{lattice} = -\frac{1}{2\nabla T} \left[\frac{\dot{Q}}{L \times t} \right] \quad (1)$$

where $\kappa_{lattice}$ is the thermal conductivity of the monolayer, ∇T is the temperature gradient established between the heat source and heat sink due to the imposed heat flux, \dot{Q} . L and t are the effective width and thickness of the suspended monolayer. Thermal conductivity is calculated for four classes of (Mo|W)Se₂ systems containing different barriers to phonon propagation, namely, pure MoSe₂ and WSe₂ crystals with no point defects or interfaces, Mo_{1-x}W_xSe₂ substitutional alloys (Figure 1b), self-similar fractal MoSe₂/WSe₂ heterostructures (Figure 1c), and periodic MoSe₂/WSe₂ superlattices with a characteristic length scale, l (Figure 1d). The random Mo_{1-x}W_xSe₂ alloy is constructed by replacing x fraction of cation sites chosen at random in the MoSe₂ lattice with W atoms. Such a random alloy configuration is consistent with real TMDC alloys synthesized by scalable techniques like chemical vapor deposition (CVD)^{26,27}. Periodic superlattices are constructed as a lattice of square WSe₂ patches of size l in the MoSe₂ matrix separated by hetero-phase interfaces along the zigzag and armchair directions. Self-similar fractal structures are constructed by substitutionally alloying W atoms in the cation sub-lattice of the MoSe₂ crystal in the form of a Sierpinski carpet. Results from these deterministic fractals are expected to hold even for random fractal structures of the same fractal dimension such as amorphous two-dimensional alloys²⁸. Both periodic superlattices and fractal heterostructures are constructed with atomically-sharp interfaces with no atomic mixing that can scatter short-wavelength phonons^{29,30}. Such epitaxial interfaces between isoelectronic materials is preferable for optoelectronic applications, since diffuse interfaces, grain boundaries, inclusions and pores can also detrimentally affect electrical transport⁵. Figure 1c represents a representative fractal structures containing four levels of self-similarity. The choice of self-similarity level also dictates the overall stoichiometry of the fractal structure. All fractal structures are constructed such that the size of the smallest feature is larger than approximately 4 nm, reflecting the limits of current patterning technologies³¹.

The average lattice strain in either the alloys or the heterostructures is less than -0.075%, reflecting the near-identical in-plane lattice constants of MoSe₂ and WSe₂ ($a(\text{MoSe}_2) = 3.289\text{\AA}$ and $a(\text{WSe}_2) = 3.286\text{\AA}$)^{32,33}. Therefore, point defects and interfacial scattering results mainly from changes in the bonding interactions and atomic masses and the potential effect of long-range disorder and strain on the measured thermal transport is negligible. Details about the molecular dynamics simulations, including development of suitable empirical forcefields and workflow are given in Section I and II of the Supporting Information.

Thermal transport in Mo_{1-x}W_xSe₂ alloys

Substitutional doping of MoSe₂ by W atoms has a significant effect on the lattice thermal conductivity. Figure 2a shows the computed lattice thermal conductivity of the monolayer Mo_{1-x}W_xSe₂ alloy as a function of substitutional doping. Even moderate doping ($x < 5\%$) leads to greater than 70% reduction in lattice thermal conductivity relative to undoped crystals. Similar results were observed in various materials³⁴⁻³⁹. Classical molecular dynamics simulations exclude electronic structure effects such as charge-transfer and charge carrier-phonon interactions, therefore the large reduction in $\kappa_{lattice}$ is attributable primarily to increased rate of point defect scattering that originates from both the mass difference and inter-atomic coupling force differences resulting in greater phonon localization and reduced mean-free paths⁴⁰⁻⁴². However, there is no noticeable change in other phonon characteristics such as phonon frequencies, group velocities and phonon density of states at low frequencies.

To quantify the phonon localization effect, we computed the phonon participation ratio P_λ for the unalloyed and defect-free MoSe₂ single crystal and the 3.7% W-doped MoSe₂ alloy (Figure 2b). The phonon participation ratio, P_λ , measures the spatial

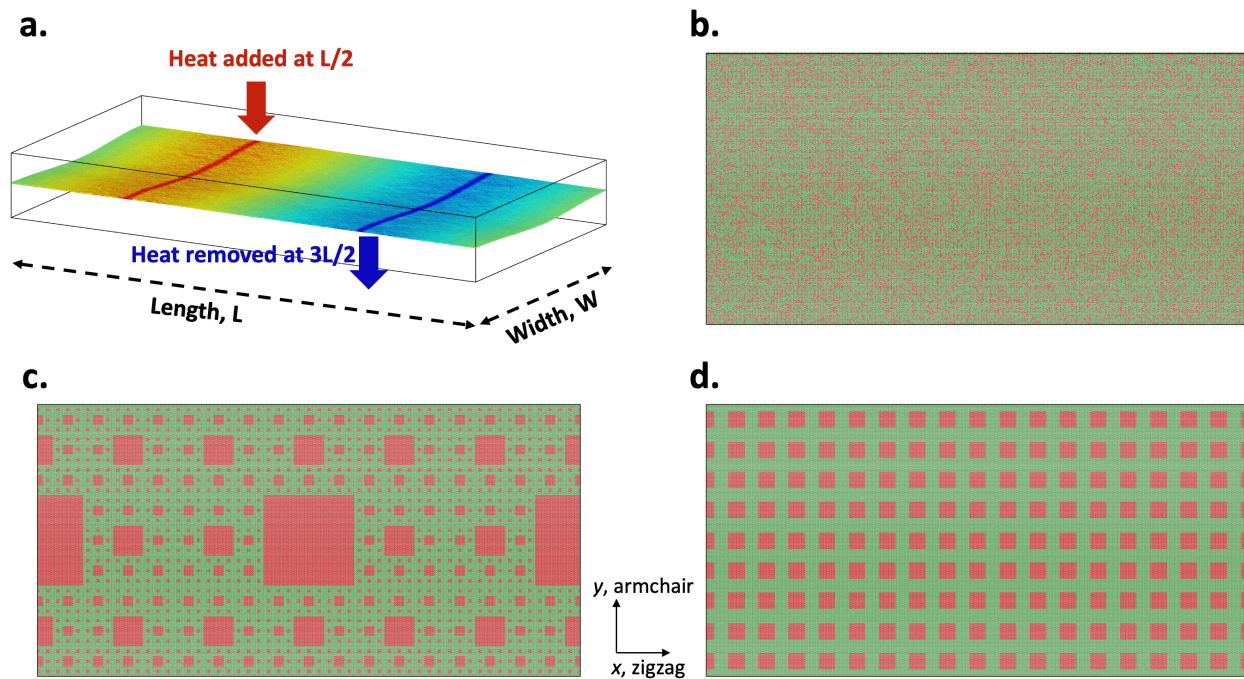


Figure 1. (a) Schematic of the thermal conductivity simulation. Heat is added at $L/2$ and removed at $3L/2$ establishing a thermal gradient between the hot and cold regions. (b-d) Different $(\text{Mo|W})\text{Se}_2$ systems with different phonon scattering features. Figure (b) shows a random distribution of WSe_2 (red) in a MoSe_2 (green) system, corresponding to a 40% distribution of WSe_2 in MoSe_2 . Figure (c) shows a level 4 fractal heterostructure and (d) shows a periodic $\text{MoSe}_2|\text{WSe}_2$ superlattice.

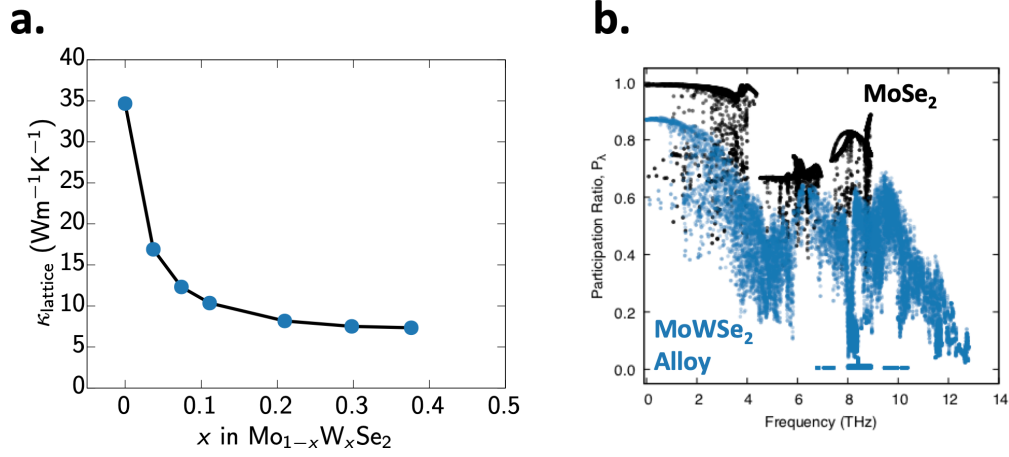


Figure 2. a) shows the variation of thermal conductivity with respect to the percentage of tungsten present in the system. b) The participation ratio of phonons in the pure and doped MoSe₂ crystals.

localization of a phonon mode, λ and it is defined as^{43,44}

$$P_{\lambda} = \frac{1}{N \sum_i \left(\sum_{\alpha} \varepsilon_{i\alpha,\lambda}^* \varepsilon_{i\alpha,\lambda} \right)^2} \quad (2)$$

where N is the total number of atoms and $\varepsilon_{i\alpha,\lambda}$ is the α^{th} cartesian component of the eigen-mode λ for the i th atom. P_{λ} is a dimensionless quantity ranging from $1/N$ to 1, with ≈ 1 denoting the propagating mode and ≈ 0 denoting the localized mode.

We observe that the degree of localization is enhanced for all phonons of finite frequency in doped MoSe₂ crystal, as shown by the lower values of P_{λ} in doped-MoSe₂ as compared to that in dopant-free MoSe₂ single crystal samples. This behavior is consistent with Anderson's theory of localization of waves in disordered two-dimensional media driven by interference between multiple wave scattering⁴⁵ as well as experimental observations in other two-dimensional materials⁴⁶. It can also be seen that substitutional point defects lead to a large suppression in thermal transport by high-frequency, low mean-free-path phonons, while long wavelength acoustic phonons undergo less scattering resulting in a finite and moderately large thermal conductivity even at high doping level. Further, it is noticeable that thermal conductivity of the alloy remains constant and relatively insensitive to W content beyond approximately 20% alloying. This low and composition-independent thermal conductivity implies that substitutional alloys are not suitable for thermal design applications.

Fractal MoSe₂|WSe₂ heterostructures

There exist several empirical models to describe transport processes (electrical, thermal and mass) in porous, self-similar and fractal media⁴⁷⁻⁴⁹. However, they provide a description of macroscopic properties of the system only in terms of the bulk properties of the individual phases, excluding any interfacial effects. The most common model for transport through irregular, porous and self-similar media is Archie's law⁵⁰. This empirical relation, given by $\dot{Q} \propto \phi^m/a$ relates flux (thermal or mass) through the medium, \dot{Q} to the phase fraction, ϕ and via the empirical exponent m which takes a value between 1.3 - 2.5 and tortuosity of the thermal path, a ⁵¹. An alternative model by Miller suggests that⁴⁹, $\sigma_{max} = 1 - \left(\frac{1}{1-2G}\right)c$, where c is the concentration of the WSe₂ phase (assumed to be of zero conductivity) and σ_{max} is the thermal conductivity of the pure MoSe₂ phase and G is some geometric parameter equal to 0.27 for square patches. Extending this thought, we can show that in a fractal of order n , the effective matrix around the largest central particle is a fractal of order $n - 1$. Therefore, we can write $\sigma_n = \sigma_{n-1} * \left(1 - \frac{1}{1-2G}\right)$. This assumption is also common in more complex models for thermal transport in regular fractal systems. However, none of these models can accurately capture the gradual, near-linear variation of $\kappa_{lattice}$ with WSe₂ phase fraction, shown in Figure 3a, because they do not consider the role of the MoSe₂|WSe₂ interfacial scattering of phonons, which is the dominant scattering mechanism in these systems and the thermal boundary resistance of the MoSe₂|WSe₂ interface, as described by the acoustic mismatch model⁵². Further, thermal transport in the resulting MoSe₂ and WSe₂ nano domains will also demonstrate significant size effects within the Casimir regime (i.e. smallest feature size < phonon mean free path). Therefore Archie's law and other previously determined models cannot be applied, contrary to the results of Ref.⁵¹.

In these self-similar structures, the reduction in thermal conductivity is caused by phonon scattering at MoSe₂/WSe₂ heterointerfaces. To understand this scattering process, we compute the time-averaged heat flux on each atom in NEMD

simulations using the expression

$$q = e \cdot v_i - S_{ij} \cdot v_j \quad (3)$$

where e , v_i , and S_{ij} are the energy, velocity vector, and local stress tensor at each atom^{53,54}. Figure 3b shows the computed per-atom flux through the fractal-patterned MoSe₂/WSe₂ heterostructure. It is noticeable that the MoSe₂/WSe₂ interfaces are the primary source of phonon scattering and that the majority of the thermal flux flows through regions of the fractal structure that contain no MoSe₂/WSe₂ interfaces in the x -direction. The figure also shows that the majority of the thermal boundary resistance is concentrated at the interfaces closest to the hot or the cold end, consistent with observations from the Si-Ge system⁵⁵.

Thermal transport in periodic superlattices

In order to understand if the inherent lack of periodicity in the fractal structure affects phonon propagation, we also compute the thermal conductivity of periodic MoSe₂|WSe₂ superlattices with square patches of WSe₂ patches embedded in a MoSe₂ matrix (Figure 1d). Specifically, we choose heterostructures of composition 29% WSe₂, equal to that in a level 3 fractal heterostructure, for our simulations. At this constant composition, we can vary the periodicity of WSe₂ patches to construct periodic heterostructures of different interfacial densities.

Figure 3d shows the near-linear decrease in the computed thermal conductivity of the three periodic heterostructures as a function of interfacial density, as seen in other semiconducting systems like Si-Ge^{20,56}. It can be observed that the computed κ_{lattice} for the third-level fractal falls in line with the trend predicted by the periodic heterostructures. This linear and inverse dependence of thermal resistance with interfacial density (and not by their relative orientations and arrangement) indicates that thermal transport in MoSe₂/WSe₂ heterostructures is dominated by conduction of incoherent phonons. The presence of interfaces and anharmonicity of the interatomic interactions lead to decoherence of phonons and their resulting particle-like behavior⁵⁷. Coherent phonons, which can traverse periodic heterostructure, but not non-periodic fractal ones⁴⁴, contribute negligibly to the calculated thermal conductivity.

Design of heterostructures for tuning lattice thermal transport

This understanding of phonon scattering by point defects (like vacancies and dopant atoms) and heterostructure interfaces provides useful design guidelines for the construction of low thermal conductivity structure. Figure 4a shows one such heterostructure which attempts to maximize both the interfacial density as well as the concentration of dopant atoms in the WSe₂ patches and the MoSe₂ matrix. This ‘doped fractal’ structure was observed to have a thermal conductivity of only 15 W/mK, which is lower than that of either the 3%-doped Mo_{1-x}W_xSe₂ alloy or the third-level fractal MoSe₂|WSe₂ heterostructure used to construct the ‘doped’ fractal structure (Figure 4b). This behavior can be explained using Matthiessen’s rule of independent scattering events, where the overall scattering rate is a sum of individual scattering rates³⁹. These simulations show that careful control over doping and heterostructure construction can be used to controllably modify thermal conductivity of (Mo|W)Se₂ monolayer single crystals.

Discussion

We have performed non-equilibrium molecular dynamics simulations using a specifically parameterized force-field to compare the thermal conductivity of suspended Mo_{1-x}W_xSe₂ alloys with periodic and fractal-patterned MoSe₂|WSe₂ heterostructures to identify the dependence of lattice thermal conductivity on dopant concentrations and interfacial densities. We show that even low dopant concentrations (< 5% doping) can strongly localize high-frequency phonons in the (Mo|W)Se₂ crystal leading to a large (> 70%) reduction in the lattice thermal conductivity. Further, this low value of κ_{lattice} is largely insensitive to dopant concentration and therefore alloying alone is not a viable strategy for controlling thermal conductivity. On the other hand, thermal transport in both periodic and fractal patterned heterostructures is dominated by incoherent phonon conduction and varies gradually and monotonically with the density of MoSe₂|WSe₂ interfaces. Thermal conductivity can be controllably tuned by constructing doped fractal heterostructures where both scattering mechanisms operate.

References

1. Kumar, A. & Ahluwalia, P. Electronic structure of transition metal dichalcogenides monolayers 1h-mx 2 (m= mo, w; x= s, se, te) from ab-initio theory: new direct band gap semiconductors. *The Eur. Phys. J. B* **85**, 186 (2012).
2. Lin, J. *et al.* Modulating electronic transport properties of mos2 field effect transistor by surface overlayers. *Appl. Phys. Lett.* **103**, 063109 (2013).
3. Sarkar, D. *et al.* Mos2 field-effect transistor for next-generation label-free biosensors. *ACS nano* **8**, 3992–4003 (2014).

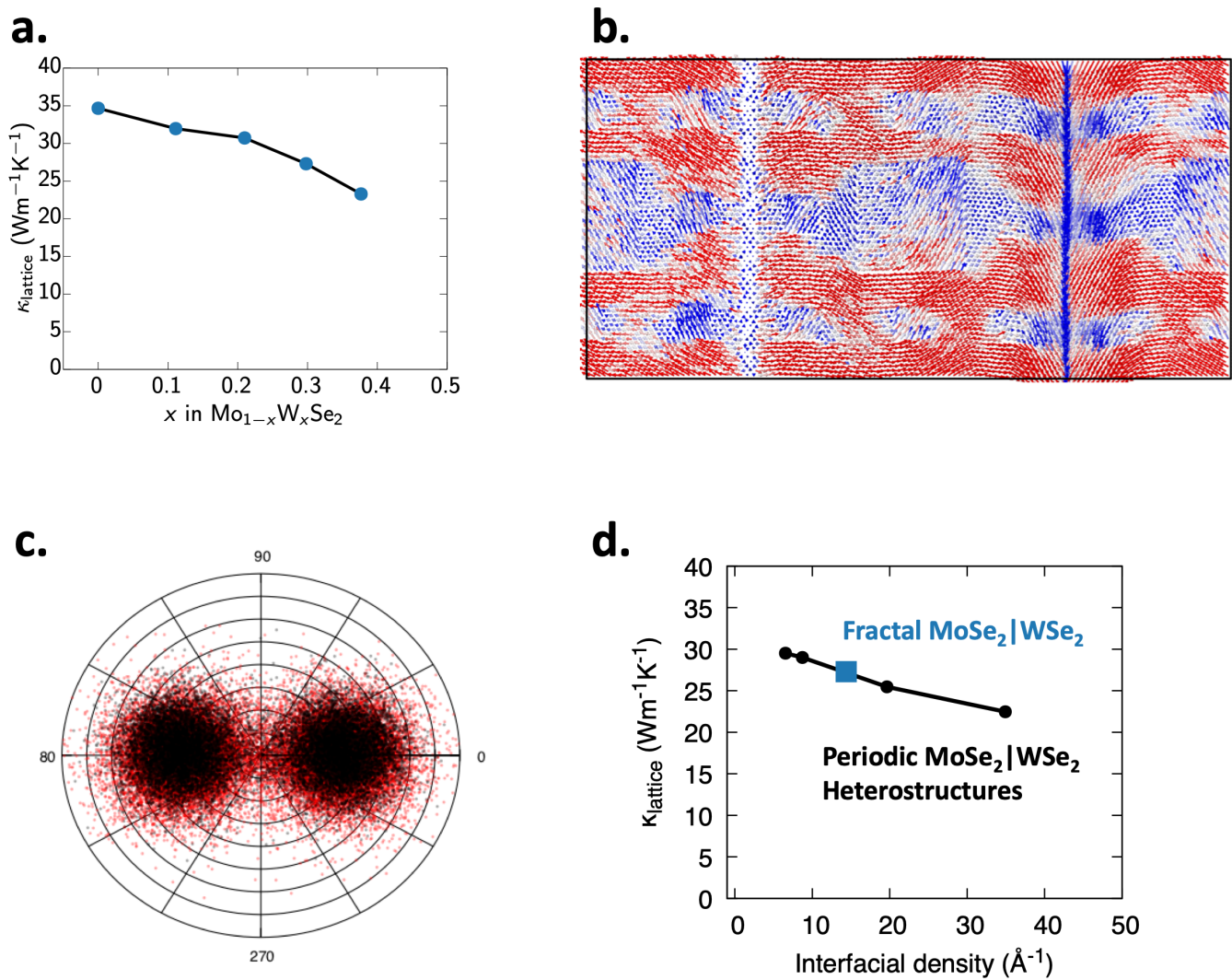


Figure 3. a) Graph showing variation of thermal conductivity in the self-similar $\text{MoSe}_2/\text{WSe}_2$ heterostructure as a function total W content. b) Shows the per-atom heat flux vectors through the second-order fractal structure, with the arrows colored by the magnitude of the heat flux in the x-direction. It is apparent that the majority of the heat flux moves through the MoSe_2 lattice and the $\text{MoSe}_2/\text{WSe}_2$ interface acts as the source of phonon scattering. (c) Angular distribution of local heat flux vectors in the pure (black) and heterostructured (red) MoSe_2 crystals. (d) Plot of thermal conductivity of periodic $\text{MoSe}_2/\text{WSe}_2$ heterostructure as a function of their interfacial density is consistent with the thermal conductivity of the fractal $\text{MoSe}_2|\text{WSe}_2$ heterostructure, showing that incoherent phonons are the dominant thermal energy carriers in these materials.

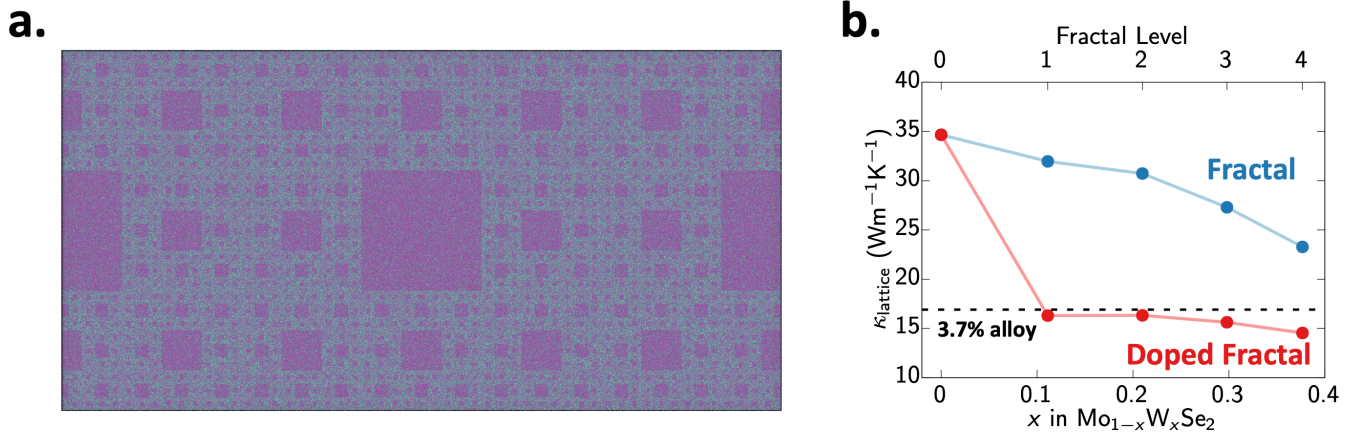


Figure 4. a) Configuration of alloyed fractal structure with 3.7% W alloying. b) The combination of two distinct phonon scattering mechanisms (i.e. interfacial formation and point defect scattering) results in a lower thermal conductivity for the alloyed fractal system (red) than can be achieved in either pure 3.7% alloying (black line) or the undoped fractals (blue)

- Wang, Q. H., Kalantar-Zadeh, K., Kis, A., Coleman, J. N. & Strano, M. S. Electronics and optoelectronics of two-dimensional transition metal dichalcogenides. *Nat. nanotechnology* **7**, 699–712 (2012).
- Sahoo, S., Gaur, A. P., Ahmadi, M., Guinel, M. J.-F. & Katiyar, R. S. Temperature-dependent raman studies and thermal conductivity of few-layer mos2. *The J. Phys. Chem. C* **117**, 9042–9047 (2013).
- Peng, B. *et al.* Thermal conductivity of monolayer mos 2, mose 2, and ws 2: interplay of mass effect, interatomic bonding and anharmonicity. *RSC Adv.* **6**, 5767–5773 (2016).
- Wang, Y., Huang, H. X. & Ruan, X. L. Decomposition of coherent and incoherent phonon conduction in superlattices and random multilayers. *Phys. Rev. B* **90**, DOI: [10.1103/PhysRevB.90.165406](https://doi.org/10.1103/PhysRevB.90.165406) (2014).
- Venkatasubramanian, R., Siivola, E., Colpitts, T. & O’Quinn, B. Thin-film thermoelectric devices with high room-temperature figures of merit. *Nature* **413**, 597–602, DOI: [Doi10.1038/35098012](https://doi.org/10.1038/35098012) (2001).
- Harman, T. C., Taylor, P. J., Walsh, M. P. & LaForge, B. E. Quantum dot superlattice thermoelectric materials and devices. *Science* **297**, 2229–2232, DOI: [DOI10.1126/science.1072886](https://doi.org/10.1126/science.1072886) (2002).
- Han, D., Ding, W., Wang, X. & Cheng, L. Tunable thermal transport in a ws2 monolayer with isotopic doping and fractal structure. *Nanoscale* **11**, 19763–19771, DOI: [10.1039/C9NR02835H](https://doi.org/10.1039/C9NR02835H) (2019).
- Zhu, T. & Ertekin, E. Phonons, localization, and thermal conductivity of diamond nanothreads and amorphous graphene. *Nano Lett.* **16**, 4763–4772, DOI: [10.1021/acs.nanolett.6b00557](https://doi.org/10.1021/acs.nanolett.6b00557) (2016). PMID: 27388115.
- Kanatzidis, M. G. Advances in thermoelectrics: From single phases to hierarchical nanostructures and back. *MRS Bull.* **40**, 687–695, DOI: [10.1557/mrs.2015.173](https://doi.org/10.1557/mrs.2015.173) (2015).
- Watanabe, T. *et al.* Thermal transport in off-stoichiometric uranium dioxide by atomic level simulation. *J. Am. Ceram. Soc.* **92**, 850–856, DOI: [10.1111/j.1551-2916.2009.02966.x](https://doi.org/10.1111/j.1551-2916.2009.02966.x) (2009). <https://ceramics.onlinelibrary.wiley.com/doi/pdf/10.1111/j.1551-2916.2009.02966.x>.
- Slack, G. A. Nonmetallic crystals with high thermal conductivity. *J. Phys. Chem. Solids* **34**, 321–335 (1973).
- Lindsay, L., Broido, D. & Reinecke, T. First-principles determination of ultrahigh thermal conductivity of boron arsenide: A competitor for diamond? *Phys. review letters* **111**, 025901 (2013).
- Mak, K. F., Lee, C., Hone, J., Shan, J. & Heinz, T. F. Atomically thin mos 2: a new direct-gap semiconductor. *Phys. review letters* **105**, 136805 (2010).
- Splendiani, A. *et al.* Emerging photoluminescence in monolayer mos2. *Nano letters* **10**, 1271–1275 (2010).
- Cao, T. *et al.* Valley-selective circular dichroism of monolayer molybdenum disulphide. *Nat. communications* **3**, 887 (2012).
- Wang, H. *et al.* Integrated circuits based on bilayer mos2 transistors. *Nano letters* **12**, 4674–4680 (2012).

20. Chen, Y. P., Deng, Z. L. & Cheng, Q. K. Thermal conductivity of si/ge nanocomposites with fractal tree-shaped networks by considering the phonon interface scattering. *Int. J. Heat Mass Transf.* **88**, 572–578, DOI: [10.1016/j.ijheatmasstransfer.2015.04.093](https://doi.org/10.1016/j.ijheatmasstransfer.2015.04.093) (2015).
21. Han, D., Fan, H., Wang, X. & Cheng, L. Atomistic simulations of phonon behaviors in isotopically doped graphene with sierpinski carpet fractal structure. *Mater. Res. Express* **7**, 035020, DOI: [10.1088/2053-1591/ab7e4b](https://doi.org/10.1088/2053-1591/ab7e4b) (2020).
22. Guo, J., Yang, F., Xia, M., Xu, X. & Li, B. Conformal interface of monolayer molybdenum diselenide/disulfide and dielectric substrate with improved thermal dissipation. *J. Phys. D: Appl. Phys.* (2019).
23. Schelling, P. K., Phillpot, S. R. & Keblinski, P. Comparison of atomic-level simulation methods for computing thermal conductivity. *Phys. Rev. B* **65**, 144306, DOI: [10.1103/PhysRevB.65.144306](https://doi.org/10.1103/PhysRevB.65.144306) (2002).
24. Cepellotti, A. *et al.* Phonon hydrodynamics in two-dimensional materials. *Nat. Commun.* **6**, 6400 (2015).
25. Lindsay, L. & Broido, D. A. Enhanced thermal conductivity and isotope effect in single-layer hexagonal boron nitride. *Phys. Rev. B* **84**, 155421, DOI: [10.1103/PhysRevB.84.155421](https://doi.org/10.1103/PhysRevB.84.155421) (2011).
26. Kochat, V. *et al.* Re doping in 2d transition metal dichalcogenides as a new route to tailor structural phases and induced magnetism. *Adv. Mater.* **29**, 1703754, DOI: [10.1002/adma.201703754](https://doi.org/10.1002/adma.201703754) (2017).
27. Apte, A. *et al.* Structural phase transformation in strained monolayer mowse2 alloy. *ACS Nano* **12**, 3468–3476, DOI: [10.1021/acsnano.8b00248](https://doi.org/10.1021/acsnano.8b00248) (2018).
28. Spagnol, S., Lartigue, B., Trombe, A. & Gibiat, V. Thermal modeling of two-dimensional periodic fractal patterns, an application to nanoporous media. *EPL (Europhysics Lett.)* **78**, 46005 (2007).
29. Luckyanova, M. N. *et al.* Coherent phonon heat conduction in superlattices. *Science* **338**, 936–939, DOI: [10.1126/science.1225549](https://doi.org/10.1126/science.1225549) (2012).
30. Luckyanova, M. N. *et al.* Phonon localization in heat conduction. *Sci. Adv.* **4**, DOI: [10.1126/sciadv.aat9460](https://doi.org/10.1126/sciadv.aat9460) (2018).
31. Chen, M., Rokni, H., Lu, W. & Liang, X. Scaling behavior of nanoimprint and nanoprinting lithography for producing nanostructures of molybdenum disulfide. *Microsystems & Nanoeng.* **3**, micronano201753, DOI: [10.1038/micronano.2017.53](https://doi.org/10.1038/micronano.2017.53) (2017).
32. Bronsema, K. D., De Boer, J. L. & Jellinek, F. On the structure of molybdenum diselenide and disulfide. *Zeitschrift fur anorganische und allgemeine Chemie* **540**, 15–17, DOI: [10.1002/zaac.19865400904](https://doi.org/10.1002/zaac.19865400904) (1986). <https://onlinelibrary.wiley.com/doi/pdf/10.1002/zaac.19865400904>.
33. Schutte, W., Boer, J. D. & Jellinek, F. Crystal structures of tungsten disulfide and diselenide. *J. Solid State Chem.* **70**, 207 – 209, DOI: [10.1016/0022-4596\(87\)90057-0](https://doi.org/10.1016/0022-4596(87)90057-0) (1987).
34. Abeles, B. Lattice thermal conductivity of disordered semiconductor alloys at high temperatures. *Phys. Rev.* **131**, 1906 (1963).
35. Tian, Z. *et al.* Phonon conduction in pbse, pbte, and pbte 1- x se x from first-principles calculations. *Phys. Rev. B* **85**, 184303 (2012).
36. Garg, J., Bonini, N., Kozinsky, B. & Marzari, N. Role of disorder and anharmonicity in the thermal conductivity of silicon-germanium alloys: A first-principles study. *Phys. review letters* **106**, 045901 (2011).
37. Daly, B., Maris, H., Nurmikko, A., Kuball, M. & Han, J. Optical pump-and-probe measurement of the thermal conductivity of nitride thin films. *J. applied physics* **92**, 3820–3824 (2002).
38. Chen, J., Zhang, G. & Li, B. W. Tunable thermal conductivity of si1-xgex nanowires. *Appl. Phys. Lett.* **95**, DOI: [10.1063/1.3212737](https://doi.org/10.1063/1.3212737) (2009).
39. Wang, Y. C., Li, B. H. & Xie, G. F. Significant reduction of thermal conductivity in silicon nanowires by shell doping. *RSC Adv.* **3**, 26074–26079, DOI: [10.1039/c3ra45113e](https://doi.org/10.1039/c3ra45113e) (2013).
40. Zhou, Z., Uher, C., Jewell, A. & Caillat, T. Influence of point-defect scattering on the lattice thermal conductivity of solid solution co (sb 1- x as x) 3. *Phys. Rev. B* **71**, 235209 (2005).
41. Fleurial, J.-P., Caillat, T. & Borshchevsky, A. Skutterudites: an update. In *Thermoelectrics, 1997. Proceedings ICT'97. XVI International Conference on*, 1–11 (IEEE, 1997).
42. Jung, G. S., Yeo, J., Tian, Z., Qin, Z. & Buehler, M. J. Unusually low and density-insensitive thermal conductivity of three-dimensional gyroid graphene. *Nanoscale* **9**, 13477–13484 (2017).

43. Bodapati, A., Schelling, P. K., Phillpot, S. R. & Keblinski, P. Vibrations and thermal transport in nanocrystalline silicon. *Phys. Rev. B* **74**, DOI: [10.1103/PhysRevB.74.245207](https://doi.org/10.1103/PhysRevB.74.245207) (2006).
44. Hu, S. Q. *et al.* Disorder limits the coherent phonon transport in two-dimensional phononic crystal structures. *Nanoscale* **11**, 11839–11846, DOI: [10.1039/c9nr02548k](https://doi.org/10.1039/c9nr02548k) (2019).
45. Anderson, P. W. Absence of diffusion in certain random lattices. *Phys. Rev.* **109**, 1492–1505, DOI: [10.1103/PhysRev.109.1492](https://doi.org/10.1103/PhysRev.109.1492) (1958).
46. Wang, Y. *et al.* Phonon lateral confinement enables thermal rectification in asymmetric single-material nanostructures. *Nano Lett.* **14**, 592–596, DOI: [10.1021/nl403773f](https://doi.org/10.1021/nl403773f) (2014).
47. Ma, Y., Yu, B., Zhang, D. & Zou, M. A self-similarity model for effective thermal conductivity of porous media. *J. Phys. D: Appl. Phys.* **36**, 2157 (2003).
48. Ma, Y., Yu, B., Zhang, D. & Zou, M. Fractal geometry model for effective thermal conductivity of three-phase porous media. *J. applied physics* **95**, 6426–6434 (2004).
49. Miller, M. N. Bounds for effective electrical, thermal, and magnetic properties of heterogeneous materials. *J. Math. Phys.* **10**, 1988–2004 (1969).
50. Archie, G. E. *et al.* The electrical resistivity log as an aid in determining some reservoir characteristics. *Transactions AIME* **146**, 54–62 (1942).
51. Thovert, J., Wary, F. & Adler, P. Thermal conductivity of random media and regular fractals. *J. applied physics* **68**, 3872–3883 (1990).
52. Cahill, D. G. *et al.* Nanoscale thermal transport. *J. Appl. Phys.* **93**, 793–818, DOI: [10.1063/1.1524305](https://doi.org/10.1063/1.1524305) (2003).
53. Hao, F., Fang, D. N. & Xu, Z. P. Mechanical and thermal transport properties of graphene with defects. *Appl. Phys. Lett.* **99**, DOI: [10.1063/1.3615290](https://doi.org/10.1063/1.3615290) (2011).
54. Kang, Y. *et al.* Thermal transport of graphene sheets with fractal defects. *Molecules* **23**, DOI: [10.3390/molecules23123294](https://doi.org/10.3390/molecules23123294) (2018).
55. Ran, X., Guo, Y., Hu, Z. & Wang, M. Interfacial phonon transport through si/ge multilayer film using monte carlo scheme with spectral transmissivity. *Front. Energy Res.* **6**, 28, DOI: [10.3389/fenrg.2018.00028](https://doi.org/10.3389/fenrg.2018.00028) (2018).
56. Abramson, A. R., Tien, C. L. & Majumdar, A. Interface and strain effects on the thermal conductivity of heterostructures: A molecular dynamics study. *J. Heat Transfer-Transactions ASME* **124**, 963–970, DOI: [10.1115/1.1495516](https://doi.org/10.1115/1.1495516) (2002).
57. Ravichandran, J. *et al.* Crossover from incoherent to coherent phonon scattering in epitaxial oxide superlattices. *Nat. Mater.* **13**, 168–172, DOI: [10.1038/Nmat3826](https://doi.org/10.1038/Nmat3826) (2014).

Acknowledgements

This work was supported as a part of the Computational Materials Sciences Program funded by the U.S Department of Energy, Office of Science, Basic Energy Sciences, under Award Number DE-SC0014607. All Simulations were performed at the Center for High Performance Computing of the University of Southern California

Author contributions statement

P.V, R.K.K and A.N conceived the simulations. A.K and N.B performed simulations and data analysis. All authors wrote and reviewed the manuscript.